SUPPLEMENTARY INFORMATION

Electrochemical gating-induced reversible and drastic resistance switching in VO_2 nanowires

Tsubasa Sasaki, Hiroki Ueda, Teruo Kanki* and Hidekazu Tanaka*

Institute of Scientific and Industrial Research, Osaka University, 8-1 Mihogaoka, Ibaraki, Osaka 567-0047, Japan

Section A. Sample preparation and pictures of devices.

VO_2 nanowire or microwire channels (w=400 nm to 3 μm) and VO_2 gates with 400-nm gaps were prepared using nano-imprint lithography. After patterning, Pt/Cr electrodes were patterned by photolithography. Using this technique, 64 nano-devices were fabricated at the same time on a 4.0-mm × 4.0-mm area, as shown in Fig S1a and b.

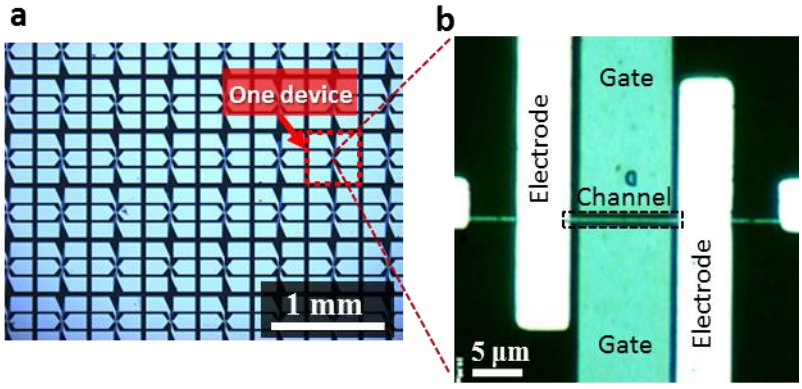

Figure S1: VO_2-based planer-gate-type electric field transistor.
a and **b**, Optical micrographs of the devices over a wide area (**a**) and a magnification of part of a device (**b**).

Section B. Static Electric Field Analysis using Finite Element Simulations

To analyze electric field distribution in the devices, numerical simulations were performed with a Finite Element Method using AMaze (Advanced Science Laboratory, Inc.). Then a three dimensional device geometry was assumed, as shown in Fig. S2a. Figure S2b shows cross-sectional potential images at the center of a device, forming the basis of Fig. 1c.

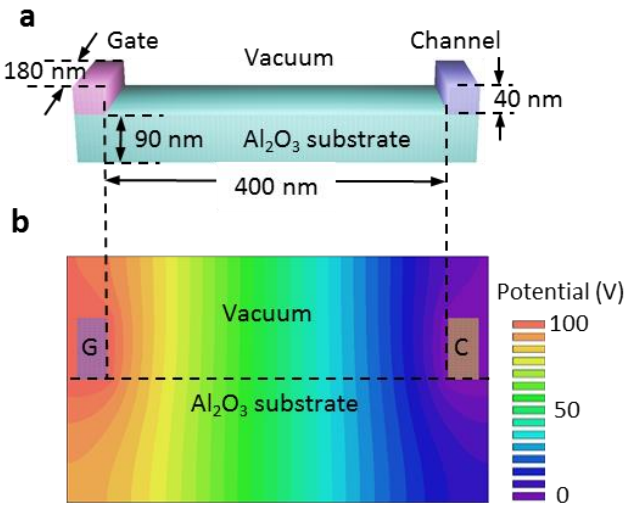

Figure S2: Device geometry used for the static-electric field simulation.
a, The device area of (x, y, z)=(500 nm, 200 nm, 200 nm), which was divided as: (dx, dy, dz)=(6 nm, 2.5 nm, 2.5 nm). The relative permittivity of Al_2O_3 is 8.5. The potential was 100 V at the gate and the channel was grounded. **b**, Cross-sectional potential map with V_G=100 V.

Section C. Resistive behavior with applied V_G=100 V and without V_G(=0 V) in 60 % humid air

Figure S3 shows time dependence of resistive behavior with V_G=100 V and 0 V in humid air condition of 60 %. We confirmed that the resistance in V_G=0 V didn't change, while that in V_G=100 V drastically reduced in the initial few minutes and gradually continue to decrease.

Figure S3: Time dependence of resistance with and without V_G (100 V and 0 V) in humid air condition.

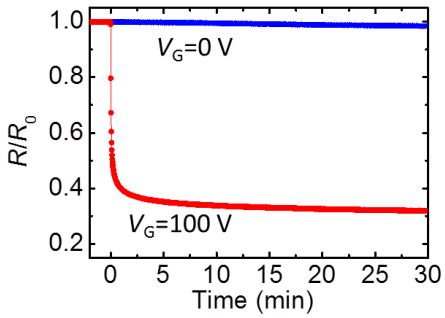

Section D. Cross-sectional elemental mapping by Tof-SIMS

To investigate the ratios of the V, O and H atoms, ToF-SIMS (time-of-flight secondary ion mass spectrometer) measurements were conducted by a technician at the Foundation for Promotion of Material Science and Technology of Japan (MST). Figure S4b–s shows the negative ion images related to V, O, H, Al and Pt, respectively, for a device with V_G=100 V. A pristine device with an area of approximately 37 μm × 37 μm, is shown in Fig. S4a. The spatial resolution and step were roughly 300 nm and 150 nm, respectively.

In the detailed analysis on the relative elemental concentrations, the cross-sectional data across the channel were sampled, indicated by the diagonal red line in Fig. S4a.

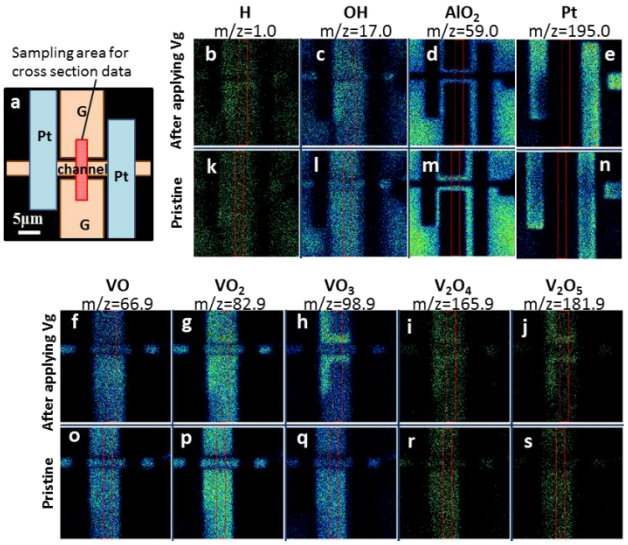

Figure S4: ToF-SIMS negative ion images of a variety of ions related to V, O, H, Al and Pt. a, Schematic of a device measured using Tof-SIMS. **b** and **k** are images for H; **c** and **l** are for OH; **d** and **m** are for AlO_2; **e** and **n** are for Pt; **f** and **o** are for VO; **g** and **p** are for VO_2; **h** and **q** are for VO_3; **i** and **r** are for V_2O_4; and **j** and **s** are for V_2O_5 in devices after applying V_G=100 V and a pristine device, respectively.

Figure S5a, b, e and f shows the intensities of each element in a device after applying V_G=100 V (a and b) and in a pristine device (e and f). Figure S5c, d, g and h shows the normalized ratios between V, H and O in a device after applying V_G=100 V (c and d) and a pristine device (g and h). From this it was identified that H increased in the channel after V_G=100 V was applied, over the standard deviation (+σ) (Fig. S5d). However, it remained almost unchanged in the pristine device (Fig. S5h).

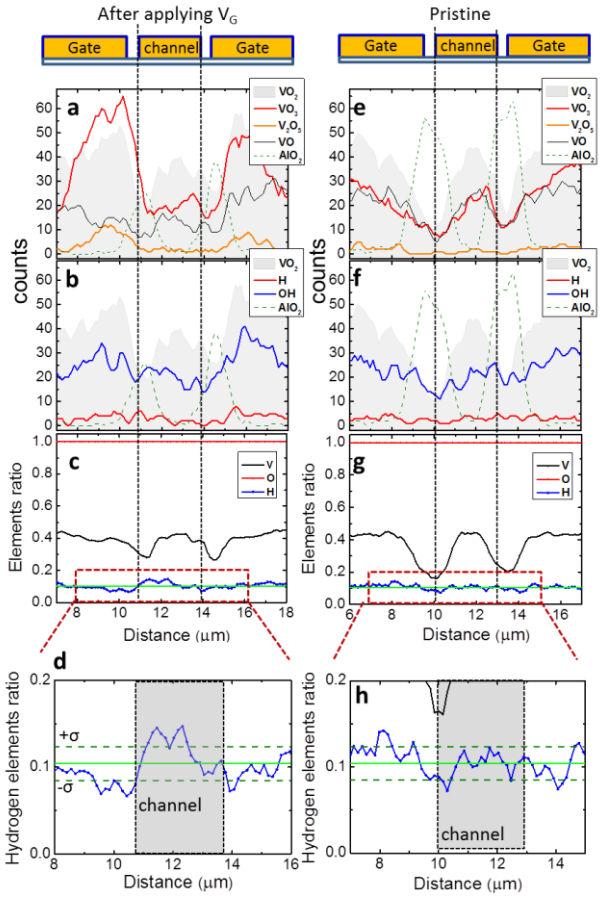

Figure S5: Cross-sectional ion maps of the images in Fig S4. a, **b**, **e** and **f**, Cross-sectional ion maps for VO_2, VO_3, V_2O_5, VO and AlO_2 in devices after applying V_G=100 V and for a pristine device, respectively. **c**, **d**, **g** and **h**, The relative elemental rates for V and H, normalized by O in a device after applying V_G=100 V and for a pristine device, respectively. The solid and dashed green lines in **d** and **h** represent the averages of the H atom profiles and the standard deviations (σ), respectively.

Section E. The natural recovery of resistance by the thermal energy

Figure S6 shows the resistance behavior in VO_2 nanowires (w=500 nm) as a function of temperature. In the resistive measurement without any V_G, the resistances between the before and after values correspond to point "A" in the inset of Figure S6. 20 minutes after applying a V_G of 100 V the resistance had reduced approximately by half, to "B" in Figure S6. This resistive state remained even following the removal of any V_G, which agrees with the behavior in Figure 2a. Thereafter, as the temperature increased to 380 K over the transition temperature without V_G, the resistance decreased accompanied by the MIT. In this process, hydrogen ions are more easily diffusible and removable from VO_2 channel with increasing temperature[17,18,21]. When the temperature returns to 290 K, the suppressed resistive state was recovered to its original state at point "A" in Figure S6.

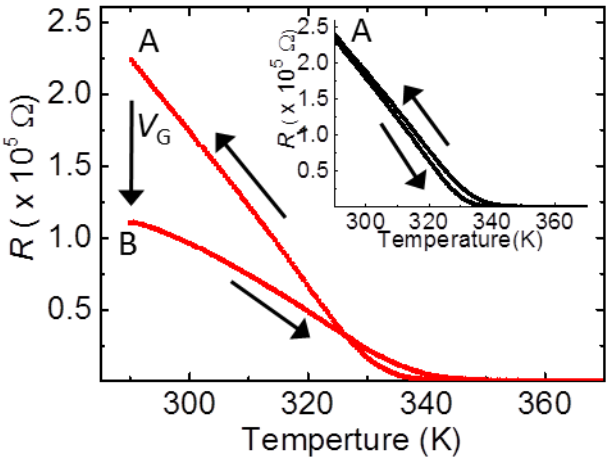

Figure S6: Temperature dependence of resistance of a VO_2 channel at V_G=0 V after applying V_G=100 V for 20 minutes at 290 K under a humidity of 50%. The inset shows the regular temperature vs resistance without V_G. The pristine resistance at 290 K is located at point "A"

Section F. Details on the calculations used to obtain Fig 4c and d.

To evaluate the time and spatial evolution of the hydrogen ion concentration in VO_2 according to equations (1) and (2), numerical analysis with the finite difference method was carried out using Mathematica 9.0. Before the calculations, equation (2) was changed to

$$\frac{\partial n^i_{HVO2}}{\partial t} = D\frac{n^{i+1}_{HVO2}-2n^i_{HVO2}+n^{i-1}_{HVO2}}{\Delta x^2} + \frac{e\mu N_0}{\varepsilon_r\varepsilon_0}\left\{\left(\frac{x_C}{\Delta x}-i\right)n^{i-1}_{HVO2} + \left(1+i-\frac{x_C}{\Delta x}\right)n^i_{HVO2}\right\}$$

, with following transformations; $\frac{\partial n_{HVO2}(x,t)}{\partial x} = \frac{n_{HVO2}(x,t)-n_{HVO2}(x-\Delta x,t)}{\Delta x}$, and $\frac{\partial^2 n_{HVO2}(x,t)}{\partial x^2} =$

$\frac{n_{HVO2}(x+\Delta x,t)-2n_{HVO2}(x,t)-n_{HVO2}(x-\Delta x,t)}{\Delta x^2}$. Then, x was replaced with $i\Delta x$, where n^i_{HVO2} and n^{i-1}_{HVO2} represent $n_{HVO2}((i\text{-}1)\Delta x,t)$ and $n_{HVO2}(i\Delta x,t)$, respectively. Thus, the numerical calculations could be performed using e=1.602×10^{-19} C and ε_0=8.859×10^{-12}. $n_{H+} = I_{gc}^{ER} \times \frac{\alpha}{S_{inter}} = 0.574V_G^2 \times \frac{\alpha}{S_{inter}}$ was obtained from Fig. S8, where S_{inter} is the number of VO_2 unit cells at the interface, written as: S_{inter}=2.691×10^6, which is the cross-sectional area where V_G was applied (35 nm × 10000 nm) divided by the volume of a VO_2 unit cell (0.4554 nm × 0.4554 nm × 0.2856 nm), α=3281 (which is a constant value that includes the intercalated rate), N_0=1.0×10^{26} m^{-3} s1, s2, ε_r=36^{s3} and E_0=2.5 × 10^6V_G V/m at the interface using the experimental parameters, and k_1=0.001, k_2=0.050 and μ=0.045 in the fitting constants from Fig 3 and Fig. 5. It was assumed that the state was completely metallic when over 2.25% of the hydrogen ions were intercalated in the region, because the resistivity in the samples underwent a change of approximately 2.25 orders of magnitude between the metallic and the insulating states at room temperature. The simulated curves in Fig 4b and c were derived using equation (3) and $\rho^i_{IH} = \rho_0 \times 10^{-n^i_{HVO2}}$. Figure S7 shows the results calculated at V_G=38 V. For this calculation, the equations were obtained from $n^0_{HVO2}(t)$ to $n^{30}_{HVO2}(t)$ as a function of time.

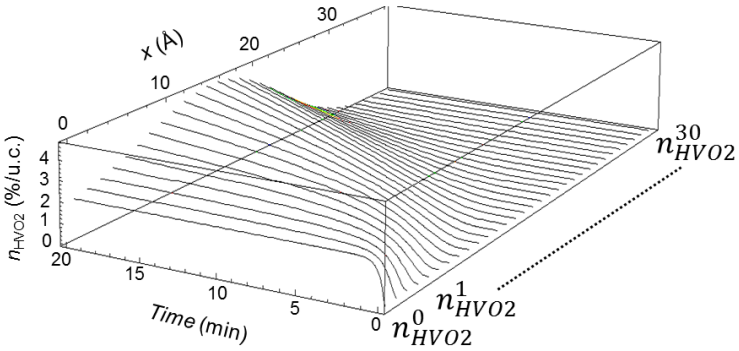

Figure S7: Simulations for the time-evolution in each n^i_{HVO2} (i=0 to 30) at V_G=38 V.

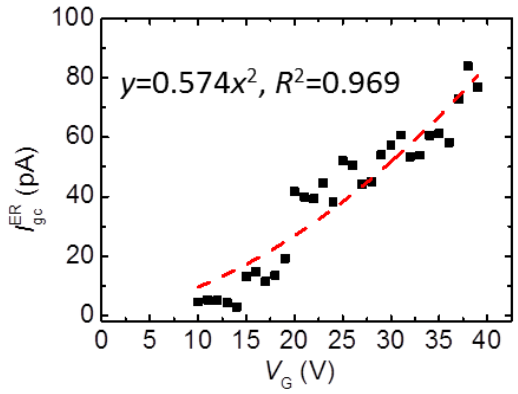

Figure S8: Current generated by the electrolysis of the adsorbed water (I^{ER}_{gc}) as a function of V_G.

Section G. Reproduction for the persisting resistance decrease after removal of the V_G in Fig.2a by this simulation.

This simulation can reproduce the persisting resistance decrease after removal of the V_G. Figure S9a shows resistance drops with time at V_G=100 V until 10 min. and at V_G=0 V over 10 min. Even following the removal of V_G the resistance continuously decreases. This behavior is due to the ion diffusion effect by the first term for concentration gradient in equation (2), though the second term can be eliminated because of V_G=0. The simulated diffusion behavior is seen in Figure S9b.

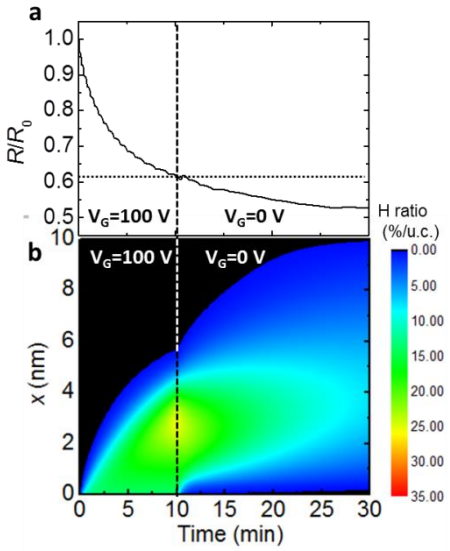

Figure S9: Time dependence of **a,** resistance and **b,** hydrogen ion diffusion behaviors at V_G=100 V and 0 V.

References

s1. Kim, H.-T.; Chae, B.-G.; Youn, D.-H. Maeng, S.-L.; Kim, G.; Kang, K.-Y.; Lim, Y.-S. *New J. Phys* **2004**, 6, 52.

s2. Ruzmetov, D.; Heiman, D.; Claflin, B., Narayanamurti, V.; Ramanathan, S. *Phys. Rev. B* **2009**, 79, 153107.

s3. Yang, Z.; Ko, C., Balakrishnan, V.; Gopalakrishnan, G.; Ramanathan, S. *Phys. Rev. B* **2010**, 82, 205101.